J. Fluid Mech. (2004), *vol.* 505, *pp.* 287–307.
DOI: 10.1017/S0022112004008523 Printed in the United Kingdom

Time-dependent fluxes across double-diffusive interfaces

By M. GRAE WORSTER

Institute of Theoretical Geophysics, Department of Applied Mathematics and Theoretical Physics, University of Cambridge, Wilberforce Road, Cambridge CB3 0WA, UK

(Received 11 July 2003 and in revised form 23 December 2003)

A simple, time-dependent model is proposed to predict the heat and salt fluxes transferred between a hot, salty fluid layer and an overlying colder, fresher fluid layer when the overall density of the lower layer is greater than that of the upper layer. The interface separating the two layers, known as a 'diffusive' interface, consists of a purely diffusing core sandwiched between vigorously convecting boundary layers. This type of interface occurs whenever the density of superposed fluid layers depends on two diffusing agents with different diffusivities such that the faster diffusing agent causes a statically unstable density variation while the slower diffusing agent causes a statically stable variation. Early experimental and theoretical studies sought a single relationship between the heat flux F_T across a diffusive interface and the buoyancy ratio $R_\rho = \beta\Delta S/\alpha\Delta T$, where ΔT and ΔS are the differences in temperature and salinity between the well-mixed fluid layers, while α and β are the coefficients of thermal and solutal expansion respectively. The model presented here supports more recent experimental findings that the relationship is time-dependent and therefore that results depend on the initial conditions and any forcing applied to the mixed regions. It is predicted that the evolution of the thickness of the core is determined principally by the mismatch between the transport rates of the slower-diffusing species (salt) diffusively from the core and convectively into the mixed regions. The introduction of time-dependence brings together the data from many previous experimental studies for both heat–salt and salt–sugar systems over a wide range of R_ρ, and both links and puts into context two previous theories of diffusive interfaces.

1. Introduction

When two agents with different molecular diffusivities, such as heat and salt, simultaneously contribute to the density of a fluid, convective motions can ensue even when the overall density field is statically stable (Turner 1974, 1979; Huppert & Turner 1981; Linden 2000). Here we are concerned with systems in which the faster-diffusing agent drives the convection, typified by the case of a warm, salty layer of water overlain by a cooler, less salty layer. It is characteristic of such systems that well-mixed layers form, separated by narrow 'diffusive' interfaces. These occur in the oceans (see the review by Schmitt 1994), for example where cold, Arctic water diluted by the spring melting of sea ice meets warmer, saltier water from the Atlantic; during replenishment of some magma chambers (Huppert 1986); and industrially in solar ponds (Newell & Boehm 1982). Of interest and concern in all these systems is the determination of the fluxes of heat and salt between the superposed layers.

Throughout this paper, I shall use the example of heat and salt in general discussions, though comparisons will also be made with salt–sugar systems, in which salt is the faster-diffusing agent and therefore plays the role of heat.

Turner (1965, 1979) used dimensional analysis to reason that the steady heat flux transferred across a diffusive interface $F_T = k(\alpha g/\kappa\nu)^{1/3}\Delta T^{4/3}F(R_\rho, \tau, \sigma)$, where k is the thermal conductivity of the fluid, α its thermal expansion coefficient, κ its thermal diffusivity, ν its kinematic viscosity, g the acceleration due to gravity and ΔT the temperature difference between the two layers. The dimensionless function $F(R_\rho, \tau, \sigma)$ depends on the buoyancy ratio $R_\rho = \beta\Delta S/\alpha\Delta T$, where $\beta\Delta S$ is the fractional change in density caused by the salinity difference ΔS between the layers, the diffusivity ratio $\tau = D/\kappa$, where D is the diffusivity of salt, and the Prandtl number $\sigma = \nu/\kappa$. Therefore, for a given physical system, for which τ and σ are constants, a single functional relationship between $F_T/[k(\alpha g/\kappa\nu)^{1/3}\Delta T^{4/3}]$ and R_ρ has been sought. Broadly speaking, there has been some support for this idea from laboratory experiments (Turner 1965; Shirtcliffe 1973; Marmorino & Caldwell 1976; Stamp *et al.* 1998) at low to moderate values of R_ρ (between $R_\rho = 1$ and $R_\rho = 10$ approximately for the heat–salt system, for example). However, Newell (1984) has shown experimentally that, at higher values of R_ρ, the fluxes can depend significantly on initial conditions and the history of the system.

It is difficult to maintain constant the value of R_ρ during an experiment, which would entail maintaining the temperature and salinity of the two fluid layers constant even as heat and salt is transferred between them. All experiments to date have been transient but it has generally been supposed that the systems evolved through a series of quasi-steady states. With this in mind, Linden & Shirtcliffe (1978) proposed a theory in which heat and salt are diffused across a stable core region between the two layers and are carried away by convective elements that periodically break away from the edge of the core. Their model, which extended ideas proposed by Howard (1964) for high-Rayleigh-number, single-component convection from a heated horizontal plate, makes a prediction for $F(R_\rho, \tau, \sigma)$ given steady conditions.

A feature of the model developed by Linden & Shirtcliffe (1978) is that it has no solution (there is no steady state) when $R_\rho > \tau^{-1/2}$. Their model centres on the idea of a cyclical process in which the boundary layers separating the diffusive core from the well-mixed layers grow by diffusion until a local Rayleigh number is exceeded, then erupt, restoring the layers to their initial state. Linden & Shirtcliffe suggest that at larger values of R_ρ the cyclical eruption cannot return the layers to their initial state and note that there must then be a build-up of heat and salt at the edges of the diffusive core which cannot be removed by convection.

The model proposed in the present paper has the same structure as that developed by Linden & Shirtcliffe but takes account of the time-dependent balance of fluxes across the boundary layers, diffusively from the core and convectively into the mixed layers. The thickness of the core region thus evolves in time. The model predicts the same steady states found by Linden & Shirtcliffe but also finds that $F(R_\rho, \tau, \sigma)$ depends on the rate of evolution towards the steady state relative to the rate at which the mixed layers evolve in transient experiments. Specifically, that F is time-dependent.

Newell (1984) performed experiments with heat and salt (for which $\tau^{-1/2} \approx 10$) for values of R_ρ ranging up to 30. He noted that the core grew at a rate commensurate with the rate of solutal diffusion and proposed a simple model in which salt transport is unaffected by any convective motions. He estimated the thickness of the core region as $h = \sqrt{\pi Dt}$, where t is time, based on the salinity gradient in the middle of a purely diffusing core, and estimated the heat flux by a linear temperature gradient across the

core. These estimations gave good qualitative agreement for the shape of $F(R_\rho, \tau, \sigma)$ at large values of R_ρ, though the predicted values were a little high compared with his experimental results. The model proposed here confirms the physical balances adopted by Newell in the high-R_ρ regime, but the detailed evolution is found to be different.

The model is described in § 2 and various asymptotic solutions are obtained in § 3 for an ideal system with initial conditions corresponding to two superposed uniform layers separated by a sharp interface. These conditions are most closely approximated in experiments (Shirtcliffe 1973; Stamp *et al.* 1998) using aqueous solutions of salt and sugar. Comparisons between the model predictions and the results of these experiments are made in § 4. Experiments using heat and salt as the diffusing agents have generally involved externally imposed heating of the lower layer or cooling of the upper layer in addition to natural heat transfer across the diffusive interface between the layers. For example, in his experiments, Turner (1965) started with an isothermal system with a salty layer below a less salty layer and proceeded to heat the lower layer. The time-dependent model developed here suggests that the heat flux across the diffusive interface during such 'run-up' experiments evolves differently than when the system runs down naturally towards an isothermal state. Comparisons with Turner's experimental results and with the run-down experiments using heat and salt of Newell (1984) are made later in § 4.

2. Formulation of the model

The model proposed consists of a horizontal core layer of fluid, across which heat and salt are transported by diffusion alone, sandwiched between two mixed layers driven by thermal convection from boundary layers at the edges of the core. The thickness of the core evolves in time in response to the mismatch between the diffusive fluxes across the core and the convective fluxes into the mixed layers. The uniform temperatures and salinities of the mixed layers are allowed to vary in time, while the diffusive profiles of temperature and salinity in the core vary in both space and time.

Consider a rectangular container half-filled with warm, salty water underlying a layer of cooler, fresher water (figure 1). The upper layer initially occupies the region $0 < z < H$ and has temperature T_0 and salinity S_0. Owing to the assumed symmetry of the system, the (*intermediate* or *interfacial*) temperature T_i and salinity S_i at the mid-plane $z = 0$ remain constant in time. For simplicity, we assume that all the physical parameters of the fluid are constant, independent of temperature and salinity.

We assume that there are two well-mixed layers, one above and one below a diffusive core of thickness $2h(t)$, where t is time. The upper mixed layer, occupying $h(t) < z < H$, has temperature $T(t)$ and salinity $S(t)$. We wish to determine the fluxes of heat and salt between the two mixed layers, i.e. the evolution of T and S, as well as the thickness and structure of the diffusive core.

Within the diffusive core we shall use the symbols $T(z, t)$ and $S(z, t)$ to denote the local temperature and salinity. These satisfy the diffusion equations

$$\frac{\partial T}{\partial t} = \kappa \frac{\partial^2 T}{\partial z^2} \qquad \text{and} \qquad \frac{\partial S}{\partial t} = D \frac{\partial^2 S}{\partial z^2}, \tag{2.1a, b}$$

with

$$T = T_i, \qquad S = S_i \qquad (z = 0), \tag{2.2}$$

$$T = T_h(t), \quad S = S_h(t) \qquad (z = h(t)), \tag{2.3}$$

where $T_h(t)$, $S_h(t)$ and $h(t)$ are to be determined.

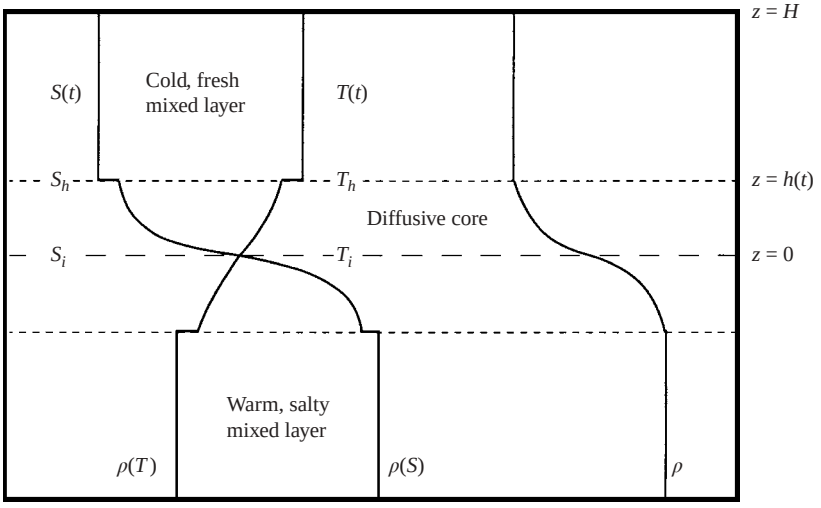

FIGURE 1. Schematic diagram of a two-layer, double-diffusive system with a cold, relatively fresh layer overlying a warmer saltier layer. The curves show the contributions $\rho(T)$ and $\rho(S)$ to the density field made by the temperature T and salinity S fields respectively, and the total density field ρ.

The temperature of the upper mixed layer evolves according to

$$\rho c_p (H-h)\frac{\mathrm{d}T}{\mathrm{d}t} = F_T, \tag{2.4}$$

where ρ is the fluid density, c_p is its specific heat capacity and F_T is the convective heat flux across the boundary layer separating the diffusive core from the well-mixed layer. In common with Linden & Shirtcliffe (1978), we assume that the boundary layer is narrow compared with the depths of both the diffusive core and the mixed layer and that therefore the heat flux F_T is independent of these depths. Dimensional analysis alone, similar to that used for high-Rayleigh-number convection from a heated, horizontal plane (Turner 1979; Linden 2000), then shows that

$$F_T = \lambda(\tau) k \left(\frac{\alpha g}{\kappa \nu}\right)^{1/3} (T_h - T)^{4/3}, \tag{2.5}$$

where $k = \rho c_p \kappa$ and $T_h - T \equiv \delta T/2$ is the temperature jump across the boundary layer.† The heat flux is affected additionally by the salinity difference across the boundary layer but by assumption (see (2.10) below) the salinity difference is linearly related to the temperature difference and the parameterization (2.5) is retained. The parameter $\lambda(\tau)$ cannot be determined from dimensional analysis but must either be determined empirically or from a local model of the convective process characterizing the boundary layer. For example, Linden & Shirtcliffe (1978), following ideas proposed by Howard (1964) for convection from a heated, horizontal plate, considered the cyclic growth by diffusion and decay by convective eruption of the boundary layer to

† More recent ideas on high-Rayleigh-number convection (e.g. Castaing *et al.* 1989) leading to a $\frac{9}{7}$ power law between heat flux and temperature jump could be incorporated here but would not significantly alter the experimental predictions made in this paper.

determine

$$\lambda(\tau) = 2^{4/3}\frac{\lambda^{SP}}{\pi^{1/3}}\left(1-\tau^{1/2}\right), \tag{2.6}$$

where $\lambda^{SP} = (1/R_c)^{1/3}$, and R_c is the critical value of the Rayleigh number at which the boundary layer breaks down, taken to be $R_c = 1629$, so that $\lambda^{SP} = 0.085$. The value of $\lambda(\tau)$ given by (2.6) will be used in § 3, where comparisons with the model of Linden & Shirtcliffe (1978) are made, but $\lambda(\tau)$ will be treated as an empirical constant (the sole adjustable parameter used to fit experimental data) in later sections, where comparisons with experiments are made.

The salinity of the upper mixed layer evolves according to

$$(H-h)\frac{\mathrm{d}S}{\mathrm{d}t} = F_S, \tag{2.7}$$

where F_S is the convective salt flux across the boundary layer. Scaling arguments based on the idea that salt is diffused into the thermal, convective elements before they break away from the boundary layer suggest that the buoyancy flux ratio

$$\beta F_S/\alpha F_T = \tau^{1/2}. \tag{2.8}$$

This expression is confirmed by the local model of Linden & Shirtcliffe (1978) and is supported well by laboratory experiments using heat and salt when R_ρ is greater than about 2 (Turner 1965) and by laboratory experiments using salt and sugar for all values of τ (Shirtcliffe 1973). Turner (1965) found that the buoyancy flux ratio increased approximately linearly from $\tau^{1/2}$ to unity as the buoyancy ratio R_ρ decreased from $R_\rho = 2$ to $R_\rho = 1$. This increase may have been a consequence of the fact that Turner was heating the lower layer, with the diffusive interface being disrupted by convective elements rising from the heated lower boundary. This will be discussed further in § 4. For now, expression (2.8) will be used universally, so that

$$F_S = \frac{\alpha}{\beta}\tau^{1/2}\lambda(\tau)\kappa\left(\frac{\alpha g}{\kappa\nu}\right)^{1/3}(T_h - T)^{4/3}. \tag{2.9}$$

The unknown functions $T_h(t)$, $S_h(t)$ and $h(t)$ are determined from conditions applied at the interface between the diffusive and convecting layers $z = h(t)$. The first condition follows from an assumption that the density field is continuous. Equivalently, it can be assumed that convective elements breaking away from the interface remove all and only the fluid that is less dense than that in the mixed layer above (Linden & Shirtcliffe 1978). These considerations give the condition

$$\alpha[T_h(t) - T(t)] = \beta[S_h(t) - S(t)]. \tag{2.10}$$

Two more conditions, expressing conservation of heat and salt at the interface, can be written as

$$(T_h - T)\dot{h} = -\kappa\left.\frac{\partial T}{\partial z}\right|_h - \frac{F_T}{\rho c_p}, \tag{2.11}$$

$$(S_h - S)\dot{h} = -D\left.\frac{\partial S}{\partial z}\right|_h - F_S, \tag{2.12}$$

where $(\cdot)$ denotes differentiation with respect to time. These last two equations represent the principal difference between the present model and that of Linden & Shirtcliffe (1978). As we shall see below, their steady-state results are recovered by setting the

left-hand sides of these equations to zero and adopting steady (linear) temperature and salinity profiles in the diffusive core.

The system of equations and boundary conditions (2.1)–(2.12) is made dimensionless by scaling lengths with $Ra^{-1/3}H$ and time with $Ra^{-2/3}H^2/\kappa$, where

$$Ra = \frac{\alpha g \Delta T H^3}{2\kappa\nu}, \tag{2.13}$$

and by writing

$$\theta = \frac{T - T_i}{T_i - T_0}, \qquad \phi = \frac{S - S_i}{S_i - S_0}. \tag{2.14a, b}$$

Note that Ra is the initial Rayleigh number characteristic of the upper layer, which has height H and a temperature contrast of $\Delta T/2 = T_i - T_0$.

With these scalings, the equations, boundary and initial conditions become

$$\frac{\partial\theta}{\partial t} = \frac{\partial^2\theta}{\partial z^2}, \qquad \frac{\partial\phi}{\partial t} = \tau\frac{\partial^2\phi}{\partial z^2} \qquad (0 \leqslant z \leqslant h(t)), \tag{2.15a, b}$$

$$\theta = \phi = 0 \qquad (z = 0), \qquad \theta = \theta_h, \quad \phi = \phi_h \qquad (z = h), \tag{2.16a–d}$$

$$\left(Ra^{1/3} - h\right)\frac{\mathrm{d}\theta}{\mathrm{d}t} = \lambda(\theta_h - \theta)^{4/3} \qquad (z > h), \tag{2.17}$$

$$\left(Ra^{1/3} - h\right)\frac{\mathrm{d}\phi}{\mathrm{d}t} = \frac{\tau^{1/2}}{R_\rho}\lambda(\theta_h - \theta)^{4/3} \qquad (z > h), \tag{2.18}$$

$$\theta = \phi = -1 \qquad (t = 0), \tag{2.19a, b}$$

$$(\theta_h - \theta)\dot{h} = -\left.\frac{\partial\theta}{\partial z}\right|_h - \lambda(\theta_h - \theta)^{4/3}, \tag{2.20}$$

$$(\phi_h - \phi)\dot{h} = -\tau\left.\frac{\partial\phi}{\partial z}\right|_h - \frac{\tau^{1/2}}{R_\rho}\lambda(\theta_h - \theta)^{4/3}, \tag{2.21}$$

$$(\theta_h - \theta) = R_\rho(\phi_h - \phi). \tag{2.22}$$

Equations (2.20) and (2.21) can be combined to give

$$\left(1 - \tau^{1/2}\right)(\theta_h - \theta)\dot{h} = -R_\rho\tau\left.\frac{\partial\phi}{\partial z}\right|_h + \tau^{1/2}\left.\frac{\partial\theta}{\partial z}\right|_h, \tag{2.23}$$

$$\left(1 - \tau^{1/2}\right)\lambda(\theta_h - \theta)^{4/3} = R_\rho\tau\left.\frac{\partial\phi}{\partial z}\right|_h - \left.\frac{\partial\theta}{\partial z}\right|_h. \tag{2.24}$$

Note, from (2.23), that $-R_\rho\phi_z \geqslant -\tau^{-1/2}\theta_z > -\theta_z$, at least when $\dot{h} > 0$, so the diffusive layer is always statically stable.

3. Theoretical results

3.1. *Numerical solutions*

Equations (2.15)–(2.19) with (2.22)–(2.24) describe a Stefan problem for the interface position $h(t)$. The diffusion equations (2.15) were solved numerically using a two-step, second-order, implicit method (Ames 1977) having first mapped the computational domain $[0, h]$ linearly onto $[0, 1]$. Simultaneously, the ordinary differential equations (2.17), (2.18) and (2.23) were solved using a second-order, Runge–Kutta method, while

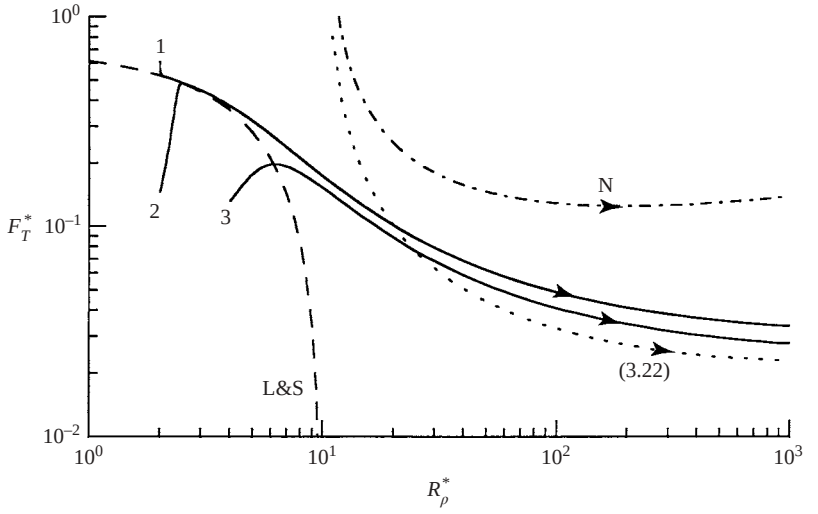

FIGURE 2. The solid curves show the evolutionary paths predicted by the present model with $\tau = 0.01$ and $Ra = 10^{10}$: 1, starting from an ideal two-layer system with no core and $R_\rho^* = 2$; 2, starting with a core of thickness $0.01Ra^{1/3}$ and $R_\rho^* = 2$; 3, starting with a core of thickness $0.01Ra^{1/3}$ and $R_\rho^* = 4$. The long-dashed curve (L&S) is the theoretical steady state for fixed R_ρ (Linden & Shirtcliffe 1978). The dot-dashed curve (N) is the prediction of the model developed by Newell (1984), while the short-dashed curve (3.22) is the result of the approximate large-time analysis given by equation (3.22). The arrows show the direction in which time is evolving.

the nonlinear equation (2.24) was solved for θ_h using a hybrid secant/binary-search method.

Figure 2 shows three calculated evolutionary paths of F_T^* versus R_ρ^*, with $\tau = 0.01$ and $Ra = 10^{10}$, where

$$F_T^* = \frac{F_T}{F_T^{SP}}, \tag{3.1}$$

and

$$F_T^{SP} = \lambda^{SP} k \left(\frac{\alpha g}{\kappa \nu}\right)^{1/3} \Delta T^{4/3} \tag{3.2}$$

is the heat flux predicted to occur across a fictitious solid conducting plate placed at the mid-plane $z = 0$, while $R_\rho^* \equiv R_\rho \phi/\theta$ is the effective buoyancy ratio between the mixed layers. For reference, the steady-state solution determined by Linden & Shirtcliffe (1978) is shown with a dashed curve. But note that steady states only exist if the properties of the mixed layers are maintained (achieved by letting $Ra \to \infty$ in the scaled equations (2.17) and (2.18)).

The first path, the solid curve labelled 1, corresponds to ideal initial conditions with $h(0) = 0$ and $R_\rho^* = R_\rho = 2$. We see that the solution decays rapidly towards the steady-state curve then evolves in a quasi-steady fashion until about $R_\rho^* = 4$. The path subsequently peels away from the steady-state curve: the dimensionless heat flux continues to decay slowly, R_ρ^* increases and the core thickens as time progresses. Figure 3 shows the dimensionless thickness of the core region as it evolves in time. Initially the core grows by solute diffusion proportional to $t^{1/2}$. The growth is arrested by the vigorous convection and is maintained at an almost constant value as the system evolves quasi-steadily. However, as R_ρ approaches and then exceeds $\tau^{-1/2}$ the

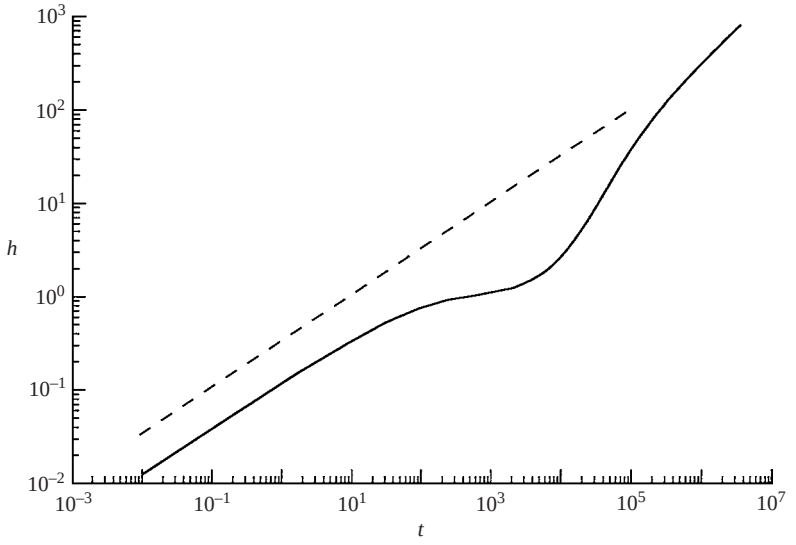

FIGURE 3. The evolution of the core thickness h with time t corresponding to the curve labelled 1 in figure 2. The dashed line has a slope of 0.5.

core thickens rapidly at first but ultimately slows to a rate a little faster than $t^{1/2}$. This structure is elucidated further below.

The second path, the solid curve labelled 2, corresponds to initial conditions with $h(0) = 0.01Ra^{1/3}$ (a core thickness of 2 mm in a tank 20 cm high, say), linear temperature and salinity profiles through the core and $R_\rho^* = R_\rho = 2$. This mimics the imperfect initial states caused by mixing during set-up of typical laboratory experiments in which the upper layer is floated onto the lower. We see that the scaled heat flux initially increases rapidly towards the steady-state curve, then crosses it and decays, following the first case closely. The initial sharpening up of the core and the corresponding increase in the vigour of convection is reported in many experimental studies.

The third path, the solid curve labelled 3, corresponds to initial conditions similar to the second case but with $R_\rho^* = R_\rho = 4$. In this case, there is no period during which the evolution is quasi-steady. The increase and subsequent decay of the scaled heat flux is found experimentally, for example by Newell (1984, his figure 5).

The approximate large-time, large-R_ρ^* predictions made by Newell (1984) and in this paper are shown in figure 2 by the dot-dashed and short-dashed curves respectively and are discussed in detail in the end of this section.

The physical mechanisms underlying the characteristics of these solutions can be described as follows. Heat is diffused across the core and into thermal boundary layers at the edge of the core. The thermal boundary layers, which are beyond the stabilizing influence of the salt field, are unstable and give rise to convective elements that break away into the mixed layers. The boundary layers are not explicitly resolved in the mathematical model but are represented by the temperature discontinuities between the core and the mixed layers. Salt is simultaneously diffused across the core, into the thermal boundary layers and is carried away by the thermal convective elements. But whereas salt diffuses independently of heat through the core, the rate at which it is transported into the mixed layers is dictated by the thermal convection. If the diffusive transport of salt exceeds the rate of its removal to the mixed layers then salt builds up at the edge of the core, stabilizing more of the thermal field, and thus the

core thickens. Conversely, when the core is initially too thick the diffusive salt flux is relatively low compared with the convective flux and the core thins.

The controlling mechanisms are further elucidated by examining the mathematical structure of the solutions in various asymptotic limits as follows. The remainder of this section is not essential to understanding the relationship between the model predictions and experimental results described in § 4.

3.2. *Behaviour at early times*

Initially, in the ideal situation, the conductive terms dominate the convective terms on the right-hand sides of equations (2.20) and (2.21), $\theta = \phi = -1$ in the mixed layer, and a similarity solution exists in the diffusive layer such that

$$\theta = \theta_h \frac{\operatorname{erf}\left(\dfrac{z}{2\sqrt{t}}\right)}{\operatorname{erf}\left(\dfrac{h}{2\sqrt{t}}\right)}, \qquad \phi = \phi_h \frac{\operatorname{erf}\left(\dfrac{z}{2\sqrt{\tau t}}\right)}{\operatorname{erf}\left(\dfrac{h}{2\sqrt{\tau t}}\right)}. \tag{3.3}$$

Substitution of these expressions into equations (2.23) and (2.24), noting that the left-hand side of (2.24) is negligible at early times, gives

$$\left(1-\tau^{1/2}\right)(1+\theta_h) = -\frac{R_\rho \phi_h}{G(\eta)} + \frac{\tau^{1/2}\theta_h}{G\left(\tau^{1/2}\eta\right)}, \tag{3.4}$$

$$0 = \frac{R_\rho \phi_h}{G(\eta)} - \frac{\theta_h}{G\left(\tau^{1/2}\eta\right)}, \tag{3.5}$$

where $\eta = h/2\sqrt{\tau t}$ is a constant and

$$G(x) \equiv \sqrt{\pi} x \mathrm{e}^{x^2} \operatorname{erf}(x). \tag{3.6}$$

Equations (3.4) and (3.5) can be rearranged, using (2.22), to give

$$\delta\theta = \frac{1}{1+G\left(\tau^{1/2}\eta\right)} \quad \text{with} \quad \frac{1+G(\eta)}{1+G\left(\tau^{1/2}\eta\right)} = R_\rho, \tag{3.7a, b}$$

where $\delta\theta \equiv \theta_h - \theta = R_\rho(1+\phi_h)$ is the scaled temperature jump at the interface between the core and the mixed layer. Note that G is a positive, monontonically increasing function and that the left-hand side of (3.7*b*) increases monotonically from 1 to infinity as η increases from zero. Therefore $\delta\theta < 1$ and (3.7*b*) always has a solution for $R_\rho > 1$, shown in figure 4. It is also interesting to note that, had we taken linear approximations for the temperature and solute fields across the diffusive layer then no root would have been found for η when $R_\rho > 1/\tau$.

Asymptotically, as $\tau \to 0$ with all other parameters of order unity, η remains of order unity, which implies that the thickness of the diffusive layer at these early times grows at a rate commensurate with solutal diffusion: in dimensional terms, $h(t) \sim 2\eta\sqrt{Dt}$. These solutions were used to initialize the numerical computations in cases when $h(0) = 0$.

3.3. *Behaviour at large times – infinite container*

As the diffusive interface thickens, the right-hand side of (2.24) diminshes and is eventually balanced by the convective flux represented by the left-hand side. If the container is sufficiently large that the temperature and salinity of the mixed regions do not change, or if external controls are put on the system so as to maintain the mixed regions at constant values then the following states are reached asymptotically

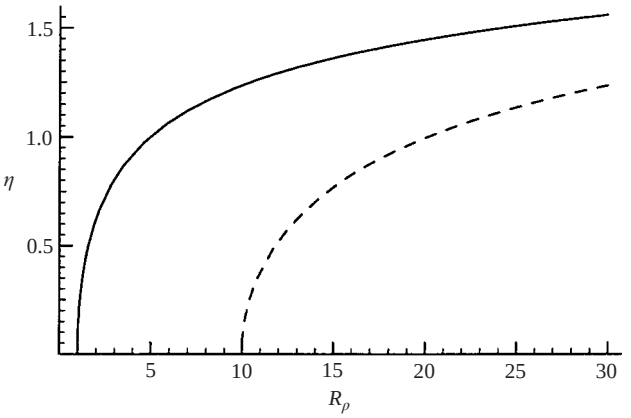

FIGURE 4. The roots of (3.7*b*) (solid curve) and of (3.14*b*) (dashed curve) as functions of R_ρ, with $\tau = 0.01$. Note that (3.14*b*) has no roots for $R_\rho < \tau^{-1/2}$.

for large time. There are two possibilities depending on the value of the buoyancy ratio R_ρ.

The case $R_\rho < \tau^{-1/2}$

In this case, analysed by Linden & Shirtcliffe (1978), a steady state can be reached. The temperature and salinity fields become linear across the diffusive interface, and equations (2.23) and (2.24) reduce to

$$0 = -R_\rho \tau \frac{\phi_h}{h} + \tau^{1/2} \frac{\theta_h}{h}, \tag{3.8}$$

$$\left(1 - \tau^{1/2}\right) \lambda (\theta_h - \theta)^{4/3} = R_\rho \tau \frac{\phi_h}{h} - \frac{\theta_h}{h}. \tag{3.9}$$

From these, we obtain the values

$$\delta\theta = \frac{1 - \tau^{1/2} R_\rho}{1 - \tau^{1/2}}, \qquad \left(1 - \tau^{1/2}\right) \lambda \delta\theta^{4/3} h = (1 - \tau R_\rho) - \left(1 + \tau^{1/2}\right)\left(1 - \tau^{1/2} R_\rho\right) \tag{3.10a, b}$$

for the dimensionless temperature jump across the boundary layer $\delta\theta$ and the thickness of the core h. It is clear that such a state can only exist for $R_\rho < \tau^{-1/2}$, otherwise $\delta\theta$ would be negative. Expression (3.10*a*) is identical to the result obtained by Linden & Shirtcliffe (1978) and gives

$$F_T^* = \frac{\lambda(\tau)}{\lambda^{SP}} \left(\frac{\delta\theta}{2}\right)^{4/3} = \frac{1}{\pi^{1/3}} \frac{\left(1 - \tau^{1/2} R_\rho\right)^{4/3}}{\left(1 - \tau^{1/2}\right)^{1/3}} \tag{3.11}$$

if expression (2.6) is used for $\lambda(\tau)$. Note that expression (3.10*a*) for $\delta\theta$ is independent of the choice of the empirical constant $\lambda(\tau)$ but the final expression in (3.11) is not.

It has been imagined by many authors that experiments and natural systems evolve through steady states, such as those described above, as the conditions of the mixed layers vary. However, this leaves open the question of how the system evolves when $R_\rho > \tau^{-1/2}$ and whether the evolution of the diffusive interface is commensurate with the evolution of the mixed layers, which would nullify the hypothesis that the system evolves through quasi-steady states, even for $R_\rho < \tau^{-1/2}$. It can be shown that the steady states are approached exponentially with a decay constant proportional to $\delta\theta^{8/3}$,

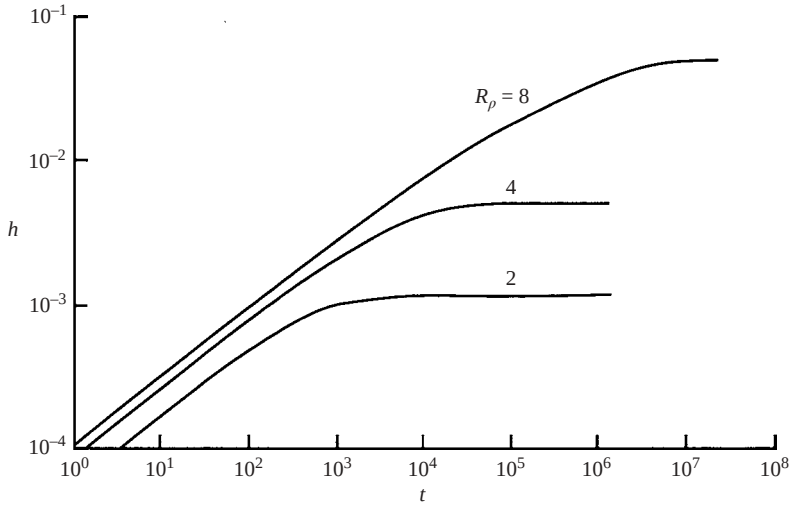

FIGURE 5. Evolution with time t of the thickness h of the diffusive core for different values of R_ρ with $\tau = 0.01$. Note that the thickness scales with $t^{1/2}$ initially but tends to its steady value exponentially with a time constant that tends to infinity as R_ρ tends to $\tau^{-1/2} = 10$.

which tends to zero rapidly as R_ρ tends to $\tau^{-1/2}$ from below. Therefore it becomes increasingly unlikely that systems can evolve through quasi-steady states as R_ρ approaches $\tau^{-1/2}$. The delay in the approach to steady state as R_ρ increases is clearly seen in figure 5, which shows examples of how the core thickness h evolves in time.

The case $R_\rho > \tau^{-1/2}$

In this case, the system runs down until $\delta\theta \ll 1$, at which stage the left-hand side of (2.23) is negligible — the accumulation of heat and salt at the interface between the diffusive and mixed regions is negligible and the fluxes across the mid-plane $z = 0$ are of similar magnitude to those into the mixed layers. There is again a similarity solution at this stage, the temperature and salinity fields being given by (3.3) with $\theta_h \approx \phi_h \approx -1$. Equations (2.23) and (2.24) become

$$0 = \frac{R_\rho}{G(\eta)} - \frac{\tau^{1/2}}{G\left(\tau^{1/2}\eta\right)}, \tag{3.12}$$

$$\left(1 - \tau^{1/2}\right)\lambda\delta\theta^{4/3}t^{1/2} = -\frac{R_\rho\tau^{1/2}\eta}{G(\eta)} + \frac{\tau^{1/2}\eta}{G\left(\tau^{1/2}\eta\right)}, \tag{3.13}$$

which can be rearranged to give

$$\lambda\delta\theta^{4/3}t^{1/2} = \frac{R_\rho\eta}{G(\eta)} \quad \text{with} \quad \frac{\tau^{1/2}G(\eta)}{G\left(\tau^{1/2}\eta\right)} = R_\rho. \tag{3.14a, b}$$

In this regime, $\delta\theta \propto t^{-3/8}$, which tends to zero as $t \to \infty$ and justifies our neglect of the left-hand side of (2.23) as well as the postulates that $\theta_h \approx \phi_h \approx -1$. Note that the heat and salt fluxes, which are proportional to $\delta\theta^{4/3} \propto t^{-1/2}$, decay with time.

The left-hand side of (3.14*b*) tends to $\tau^{-1/2}$ as $\eta \to 0+$ and increases monotonically to infinity as $\eta \to \infty$. Therefore, equation (3.14*b*) has a solution for all values of $R_\rho > \tau^{-1/2}$. This is illustrated in figure 4, which also shows that the value of η in this long-time asymptotic state is smaller than the value of η obtained initially.

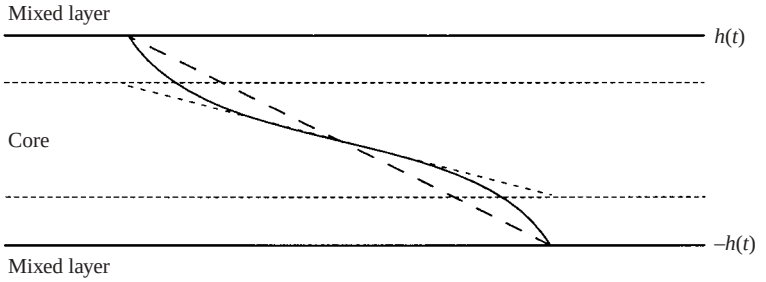

FIGURE 6. Self-similar profiles of temperature (long-dashed curve) and salinity (solid curve) within the diffusive core (bounded by horizontal solid lines) at $R_\rho = 30$, $\tau = 0.01$. The short-dashed curve shows the linear salinity profile assumed by Newell (1984) to estimate the thickness of the core, shown by horizontal dashed lines.

Asymptotic, self-similar profiles of the temperature and salinity fields when $R_\rho = 30$ are shown in figure 6. It can be seen that, whereas the temperature field is almost linear, the salinity field is not. In developing an approximate model of the evolution of the diffusive core, Newell (1984) estimated the thickness of the core based on an assumed linear salinity gradient, as shown in the figure. This underestimates the thickness of the core, which leads to an overestimate of the heat flux (see later). It is interesting to note that the maximum curvature of the salt field occurs inside the diffusive core at these large values of R_ρ, which may have caused the apparent double-boundary-layer structure visualized by Fernando (1989) using the shadowgraph technique.

3.4. *Approximate behaviour at large times — finite container*

The solutions found in the previous section for an 'infinite' container apply in a finite container for dimensionless times less than $O(Ra^{1/3})$, which corresponds to dimensional times of $O(Ra^{-1/3}H^2/\kappa)$, i.e. much shorter than the thermal diffusion time across the mixed layers. For times longer than this, equations (2.17) and (2.18) come into play, describing the evolution of the temperature and salinity of the mixed layer. These equations can be combined to show that

$$\frac{\mathrm{d}\phi}{\mathrm{d}\theta} = \frac{\tau^{1/2}}{R_\rho} \Rightarrow \phi + 1 = \frac{\tau^{1/2}}{R_\rho}(\theta + 1). \tag{3.15}$$

Because $\tau^{1/2} < 1$ and $R_\rho > 1$, this shows that the effective buoyancy ratio between the mixed layers $R_\rho^* \equiv R_\rho\phi/\theta$ increases with time (indicated by the arrows on the numerical solutions displayed in figure 2), to infinity as $\theta \to 0$. Therefore, at sufficiently large times an isolated system will find itself in the second regime ($R_\rho^* > \tau^{-1/2}$) of the previous section. The same balances apply in the interfacial conservation equations (2.23) and (2.24), which now suggest that

$$\frac{\tau^{1/2}G(\eta)}{G\left(\tau^{1/2}\eta\right)} = R_\rho^* \equiv R_\rho\phi/\theta, \qquad \lambda\delta\theta^{4/3}t^{1/2} = -\frac{\tau^{1/2}\eta}{G\left(\tau^{1/2}\eta\right)}\theta. \tag{3.16a, b}$$

For large R_ρ^*, η is a slowly varying function of R_ρ^* (it has only logarithmic dependence). We can construct an approximate solution by treating η as a constant (a slowly varying parameter of time) and use (3.16*b*) in equation (2.17) to show that

$$Ra^{1/3}\frac{\mathrm{d}\theta}{\mathrm{d}t} = -\frac{\tau^{1/2}\eta}{G\left(\tau^{1/2}\eta\right)}\frac{\theta}{t^{1/2}}. \tag{3.17}$$

Note that, though η depends only logarithmically on R_ρ^*, R_ρ^* depends exponentially on time, so the procedure followed in this subsection is not formally self-consistent and the results obtained are not asymptotic. However, the physical ideas underlying and exposed by this approximate analysis are the appropriate ones. Equation (3.17) is readily integrated to give

$$\theta \sim -\exp\left[-\frac{2\tau^{1/2}\eta}{Ra^{1/3}G\left(\tau^{1/2}\eta\right)}t^{1/2}\right]. \tag{3.18}$$

In the limit $\tau \to 0$, η remains of order unity, as we have seen, and we can simplify the expression for the temperature of the mixed layer to

$$\theta \sim -\exp\left[-\frac{t^{1/2}}{Ra^{1/3}\tau^{1/2}\,\eta}\right]. \tag{3.19}$$

This suggests that the temperatures of the mixed layers become almost equal after a dimensionless time of $O(Ra^{2/3}\tau)$, which corresponds to a dimensional time of $O(\tau H^2/\kappa)$. The system runs down on a diffusive timescale but with an effective thermal diffusivity of κ^2/D, which is greater than both of the molecular diffusivities. Note also that, in consequence of the still vigorous convection in the mixed layers, their mean temperatures are uniform rather than having the curved profiles typical of a purely diffusing system. In dimensional terms, the long-time decay of the temperature in the double-diffusive system is given by

$$\theta \sim \theta(t) = -\exp\left[-\frac{(\kappa^2 t/D)^{1/2}}{\eta(R_\rho^*)\,H}\right], \tag{3.20}$$

whereas in a purely diffusing system it is given by

$$\theta \sim \theta(z,t) = -\sin\left(\frac{\pi}{2}\frac{z}{H}\right)\exp\left[-\frac{\pi^2\kappa t}{4H^2}\right]. \tag{3.21}$$

Equation (3.18) can be combined with equations (3.15) and (3.16) to show that

$$\begin{aligned} F_T^* &\equiv \frac{\lambda(\tau)}{\lambda^{SP}}\left(\frac{\delta\theta}{-2\theta}\right)^{4/3} \\ &= \left[\lambda^{SP}\frac{G^2\left(\tau^{1/2}\eta\right)}{\tau\eta^2}H\ln\left(\frac{R_\rho^*-\tau^{1/2}}{R_\rho-\tau^{1/2}}\right)\right]^{-1}\left[\frac{\beta g\Delta S(-\phi)}{\kappa\nu}\right]^{-1/3}(R_\rho^*)^{1/3} \\ &\sim \left[\lambda^{SP}4\eta^2 H\tau\ln\left(\frac{R_\rho^*}{R_\rho}\right)\right]^{-1}\left[\frac{\beta g\Delta S(-\phi)}{\kappa\nu}\right]^{-1/3}(R_\rho^*)^{1/3} \quad \text{as} \quad \tau\to 0. \end{aligned} \tag{3.22}$$

This expression is equivalent to equation (3.3) of Newell (1984) apart from the numerical factor $4\eta^2$ in place of π, which results from the different estimations of the core thickness.†

This approximate solution and that of Newell (1984) are shown in figure 2. As suggested by figure 6, the numerically calculated heat flux is somewhat lower than that predicted by Newell owing to the fact that a linear salt profile underestimates the thickness of the core. Note that both Newell's solution and the solution given

† The factor $\pi^{3/2}$ in expression (3.3) of Newell (1984) should be replaced by π. Newell estimates the core layer thickness as $2\sqrt{\pi Dt}$, which is equivalent to taking $\eta = \sqrt{\pi}/2$.

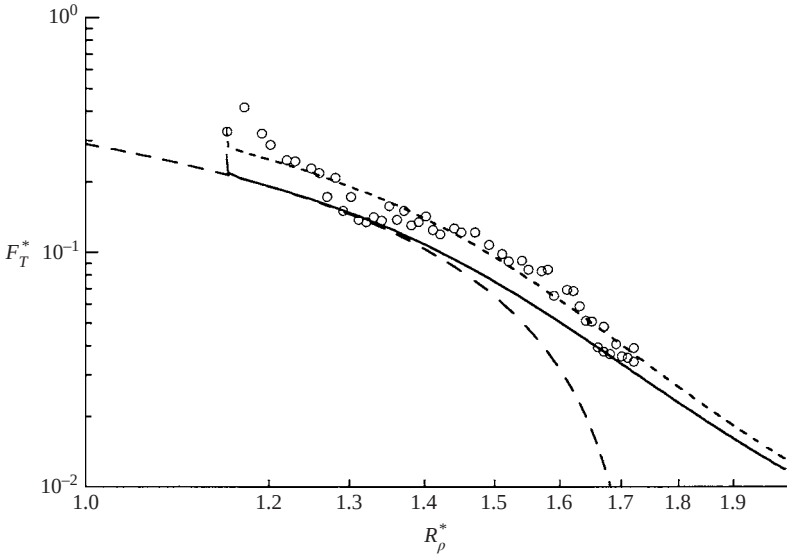

FIGURE 7. The circles show data from Run 2 of Stamp *et al.* (1998) using aqueous solutions of salt and sugar. The solid curve shows the predictions of the present model with $\lambda(\tau) = 0.062$ given by equation (2.6). The short-dashed curve is a prediction made using $\lambda(\tau) = 0.081$. The long-dashed curve is the theoretical steady state for fixed R_ρ^* (Linden & Shirtcliffe 1978). Data kindly supplied by G. O. Hughes.

in (3.22) begin to increase at large values of R_ρ^*, though the start of the increase is delayed in the latter. The numerical solution (which has been extended much further than shown) appears to decay monotonically.

4. Comparisons with experiments

4.1. *A run-down experiment using salt–sugar*

The model presented so far assumes initial conditions corresponding to two uniform superposed fluid layers with a sharp interface between them of zero thickness. It is impossible to set up such an initial condition in the laboratory but a close approximation to it can be achieved using two slowly diffusing agents, such as salt and sugar. A second advantage of using two solutes rather than heat and a solute is that an experimental tank is impermeable to the solutes but is difficult to insulate thermally. Such experiments were performed by Shirtcliffe (1973) and more recently by Stamp *et al.* (1998). All the experiments reported by these authors were for a small range of buoyancy ratios, $1 < R_\rho < 2$, that did not extend far beyond the critical value $R_\rho = \tau^{-1/2} \approx 1.74$. Stamp *et al.* (1998), after correcting an error of scaling made by Shirtcliffe (1973), have shown that the two sets of experimental studies produce similar results for the fluxes. In what follows, I have made a comparison with data from Stamp *et al.* (1998), to which I was given direct access, but the comparisons apply equally to the results of Shirtcliffe (1973).

Data from Run 2 of Stamp *et al.* (1998) are shown in figure 7, where they are compared with predictions of the present model. The solid curve shows a prediction made using the value of $\lambda(\tau) = 0.062$ given by equation (2.6) with $\tau = 0.33$. The other parameter values used in the simulation were $R_\rho = 1.15$ and $Ra = 2.3 \times 10^{11}$. The physical parameter values used in estimating the Rayleigh number were $\alpha \Delta T = 0.03$,

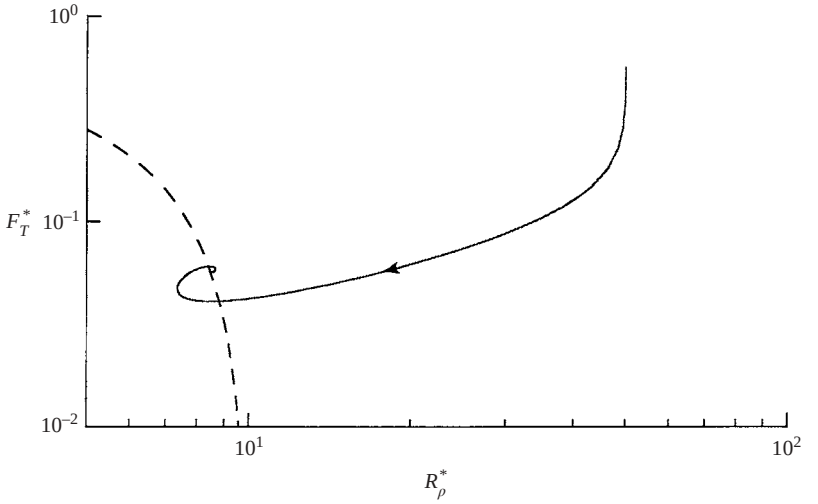

FIGURE 8. Evolution of the scaled heat flux F_T^* and the buoyancy ratio R_ρ parameterized by time, starting with $R_\rho = 50$ in a system heated from below. After some oscillations, the system settles to a point on the branch of steady states predicted by Linden & Shirtcliffe (1978), shown with a dashed curve. The arrow shows the direction in which time is evolving.

$H = 12\,\text{cm}$, $\kappa = 1.1 \times 10^{-5}\,\text{cm}^2\,\text{s}^{-1}$ and $\nu = 1.0 \times 10^{-2}\,\text{cm}^2\,\text{s}^{-1}$, where here $\alpha\Delta T$ represents the relative density contrast due to salt and κ is the diffusivity of salt. A slightly better fit to the data can be achieved using a higher value for λ. For example, the short-dashed curve in figure 7 shows a prediction made using $\lambda = 0.081$. The higher fluxes indicated by a larger value of λ may be a consequence of interfacial waves (Turner & Chen 1974; Stamp *et al.* 1998). Since the structure and amplitude of the waves vary with R_ρ, it is likely that any parametrization of λ should depend on R_ρ as well as τ.

There is some scatter in the data but nevertheless an indication that the data lie on or above the steady-state curve (long-dashed curve) and tend away from it at higher values of R_ρ, in accord with the theoretical predictions. In the narrow range of buoyancy ratio explored in salt–sugar systems, the scaled heat flux F_T^* does not deviate very far from the steady-state value determined by Linden & Shirtcliffe (1978). As we have seen, much larger deviations are to be expected at larger values of R_ρ.

4.2. *A thermal run-down experiment*

Newell (1984) performed a number of run-down experiments at high values of R_ρ using heat and salt, though none of them began from the ideal initial state that has been assumed in the paper so far. His experiments were set up by superposing two layers of different salinities but identical temperatures then heating the lower layer rapidly until the desired 'initial' buoyancy ratio R_ρ was reached. The heating was then turned off and the subsequent evolution of the system monitored. Though Newell records the measured interface thickness and the temperatures and salinities of the mixed layers at the start of each experiment, these are insufficient to initialize the model equations since the internal structure of the core depends on its history during set up.

An example of such a history is shown in figure 8. Rather than starting with $R_\rho = \infty$, as would be the case at the beginning of Newell's set-up procedure, the simulation begins with ideal superposed layers at $R_\rho = 50$ and equation (2.17) is modified by the

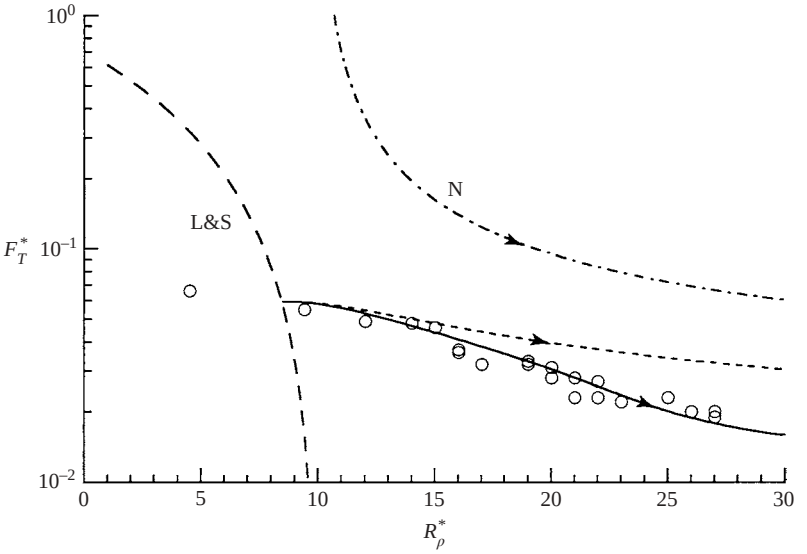

FIGURE 9. The circles show the evolutionary path of experiment 5 of Newell (1984). The solid curve and the short-dashed curve show the predictions of the present model respectively with and without account being taken of heat losses to the laboratory. The long-dashed curve (L&S) shows the steady-state prediction of Linden & Shirtcliffe (1978), while the dot-dashed curve (N) shows the prediction of the approximate model developed by Newell (1984). Data kindly supplied by T. A. Newell from the Master's thesis of Paul von Driska (1982).

addition of a heating term on the right-hand side. The simulation eventually tends towards the steady state determined by Linden & Shirtcliffe (1978), when the applied heat flux exactly balances the heat transfer across the diffusive interface. It seems that Newell began his experiments before such a steady state was reached, below and to the left of Linden & Shirtcliffe's curve. However, the steady state gives a precise initial condition and is therefore used below in the numerical simulation of the experiment.

The data in figure 9 show the evolution of experiment 5 of Newell (1984) in comparison with the models of Linden & Shirtcliffe (1978), Newell (1984) and the prediction of the present model. Parameter values used in the present simulation were $\tau = 0.01$, $Ra = 1.1 \times 10^{11}$ and $R_\rho = 8.5$. The values used in estimating the Rayleigh number were $\alpha = 3 \times 10^{-4}\,\mathrm{K}^{-1}$, $g = 980\,\mathrm{cm\,s}^{-2}$, $\Delta T = 4.9\,\mathrm{K}$, $H = 120\,\mathrm{cm}$, $\kappa = 1.46 \times 10^{-3}\,\mathrm{cm}^2\,\mathrm{s}^{-1}$ and $\nu = 0.8 \times 10^{-2}\,\mathrm{cm}^2\,\mathrm{s}^{-1}$. Using these values of τ and R_ρ, the temperature and salinity fields in the core were initialized with linear profiles given the values of $\delta\theta$ and h from (3.8). The value of $\lambda(\tau) = 0.13$ used to produce the short-dashed curve is that given by equation (2.6).

We see that the predicted evolution drifts away from the experimental data up to a factor of almost 2 in the value of F_T^*. A more significant discrepancy is that the evolutionary path indicated by the short-dashed curve takes less than 4 days to reach $R_\rho^* = 30$, whereas the experiment took about 13 days. This is evident from figure 10, which shows the thickness of the diffusive core as a function of time.

However, whereas the model assumes a perfectly insulated system, there was some heat lost to the environment during the experiment. This can be seen in figure 11, which shows the average temperature T_A in the experiment as a function of time. The data in figure 11 are represented well by an exponential function of the form

$$T_A = T_1 + T_2 \exp(-m^* t),$$

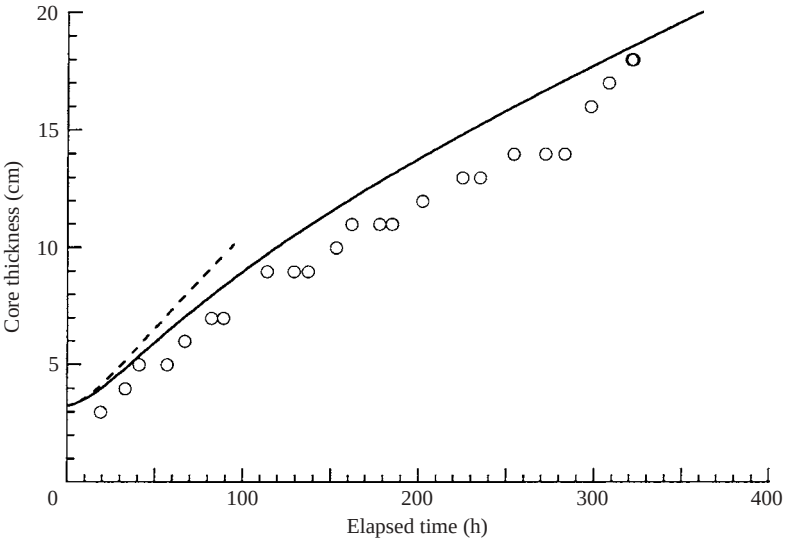

FIGURE 10. The circles show the core thickness measured in experiment 5 of Newell (1985). The solid curve and the short-dashed curve show the predictions of the present model respectively with and without account being taken of heat losses to the laboratory. Data kindly supplied by T. A. Newell from the Master's thesis of Paul von Driska (1982).

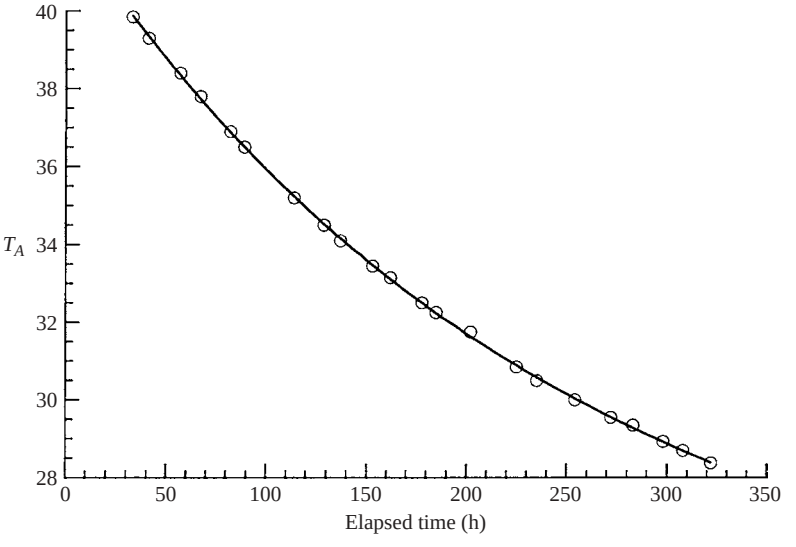

FIGURE 11. The circles show the average temperature T_A in experiment 5 of Newell (1984) as a function of time. The curve shows the best fit to a curve of exponential form. Data kindly supplied by T. A. Newell from the Master's thesis of Paul von Driska (1982).

where

$$T_1 \approx 23.2^\circ\mathrm{C}, \qquad T_2 \approx 19.1^\circ\mathrm{C} \qquad \text{and} \qquad m^* = 1.12 \times 10^{-6}\,\mathrm{s}^{-1},$$

as shown. If we assume that a fraction f of the heat lost to the environment is lost from the upper mixed layer and a fraction $1 - f$ is lost from the lower mixed layer

then equation (2.17) is modified by an additional term on the left-hand side to become

$$\left(Ra^{1/3} - h\right)\frac{\mathrm{d}\theta}{\mathrm{d}t} = \lambda(\theta_h - \theta)^{4/3} + \frac{2T_2}{\Delta T}(1-2f)Ra^{1/3}\, m\mathrm{e}^{-mt}, \tag{4.1}$$

where $m = m^* Ra^{-2/3} H^2/\kappa$. A value of $f = 0.56$ was used to produce the solid curves in figures 9 and 10, where it can be seen that much better agreement between theory and experiment can be achieved by taking such heat losses into account. In particular, the evolutionary path in (R_ρ^*, F_T^*)-space is now predicted to take about 13 days, in agreement with the experiment. It is not unreasonable that slightly more heat was lost from the upper layer, which had less insulation on its upper surface than the base. The fact that the prediction of core thickness is a little higher than that measured may be a consequence of the initial conditions used or of the way in which the core thickness was measured by extrapolating the approximately linear temperature field at the centre of the core (see figure 6).

The quantitative comparisons should be treated with a little caution because some discrepancies may also be attributable to the variations of the physical parameters with temperature, not accounted for in the theoretical prediction. For example, the variations of the thermal expansion coefficient α and the kinematic viscosity ν cause the Rayleigh number Ra to vary by a factor of almost 3 and $Ra^{1/3}$ to vary by 40% over the temperature range of the experiment (between 20°C and 40°C). However, the comparisons shown seem to indicate that good predictions should be possible if careful attention is paid to parameter values and a full heat budget.

4.3. *Forced experiments*

Turner (1965) performed a number of experiments in which a two-layer system, initially isothermal with a less salty layer above a saltier one, were forced with a constant heat flux through the lower boundary. The temperatures and salinities of the two layers were measured as they evolved in time, and from these measurements the heat and salt fluxes across the interface between the two layers were determined. The model proposed by Linden & Shirtcliffe (1978) gave predictions that seemed to give the wrong trend in comparison with the data, as shown by the dashed curve in figure 12, casting some doubt on the structure of their model and the physical mechanisms it embodied. However, as shown by the solid curve in figure 12, the steady states predicted by the present model, which has the same basic structure as Linden & Shirtcliffe's model, fit Turner's data well in the range $R_\rho^* > 3$ if the constant of proportionality in the four-thirds law applied to the thermal boundary layers bounding the diffusive core is taken to be $\lambda(\tau) = 0.075$. The details of cyclic eruption of the thermal boundary layers employed by Linden & Shirtcliffe serve only to provide an estimate of $\lambda(\tau)$, which, as suggested in § 2, should be treated as an empirical constant. I therefore believe that a different interpretation of the experiments is possible as follows.

The heating applied during Turner's (1965) experiments would have driven turbulent, convective motions in the lower layer. At the higher values of R_ρ^*, those motions may have been insufficient to disrupt the structure of the diffusive core, which would have therefore evolved as described in this paper. Simulations such as that shown in figure 8, using heating rates equal to those applied by Turner (1965), predict that the steady-state curve is reached after only a few minutes (real time) and the system subsequently evolves quasi-steadily along that curve. At lower values of the buoyancy ratio R_ρ^* (below about 3 in these particular experiments), the turbulence in the lower layer driven by the heating elements may have actively eroded the lower

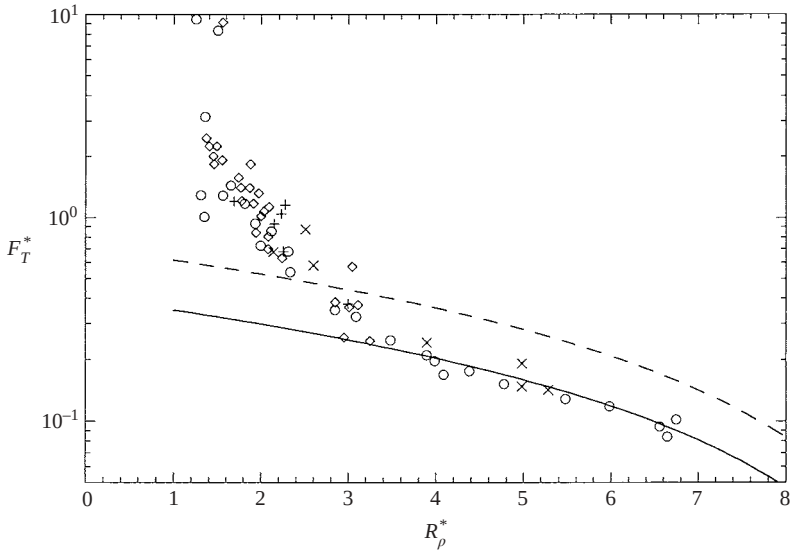

FIGURE 12. The data points show the scaled heat fluxes measured by Turner (1965), with the different symbols corresponding to the different heat fluxes applied to the lower layer. The solid curve shows the steady-state result of the present model when $\lambda(\tau) = 0.075$, while the dashed curve shows the result of Linden & Shirtcliffe (1978), which has $\lambda(\tau) \approx 0.13$ when $\tau = 0.01$.

edge of the core or generated interfacial waves or both. Either of those mechanisms would enhance the heat transfer across the core relative to that predicted by the present model and might explain the deviation between data and theory shown in figure 12. The fact that the salt/heat flux ratio in Turner's experiments remained constant, and approximately equal to $\tau^{1/2}$ for R_ρ^* down to about 2, suggests that in the range $2 < R_\rho^* < 3$ in Turner's experiments, the core was not totally disrupted, and the physical mechanisms described in § 3 were dominant in controlling the heat and salt transport between the core and the upper mixed layer. Finally, when $R_\rho^* < 2$ in Turner's experiments, the turbulence in the lower layer may have been sufficient to disrupt the core entirely and cause direct turbulent entrainment of the upper layer, as suggested by Linden (1974). If these pictures are correct then the transitions between the different sorts of behaviour would depend critically on the strength and nature of any convection externally driven in either of the mixed layers. That this may be the case is suggested by the very large scatter in the data obtained by Turner (1965) for $R_\rho^* < 3$.

5. Conclusions

A new, time-dependent model of double-diffusive interfaces has been developed which codifies many existing ideas about their structure. The model and its solutions give a clear physical picture of the dynamics of double-diffusive interfaces and quantify their evolution and the fluxes of heat and salt transported across them. Briefly, heat diffused across the interface drives vigorous thermal convection in the mixed layers either side of it, while the mismatch between the rates at which salt is diffused across it and is carried away by the thermal convective elements determines the evolution of its thickness. The new model reproduces in essence the steady-state model of Linden &

Shirtcliffe (1978) at low buoyancy ratios and the approximate time-dependent model of Newell (1984) for high buoyancy ratios.

Predictions of the model have been compared with three previous experimental studies: a run-down experiment with salt and sugar (Stamp *et al.* 1998); a run-down experiment with heat and salt (Newell, 1984); and a forced experiment in which a two-layer, salt-stratified system was heated from below (Turner 1965). Although precise comparisons are hampered by the lack of knowledge of the initial conditions and because variations of physical properties with temperature were not taken into account, good agreement between theory and exeriment was obtained in all cases.

When the buoyancy ratio $R_\rho < \tau^{-1/2}$ and the mixed layers have constant properties then a steady state is possible in which the heat flux across the interface is

$$F_T = \lambda(\tau) \left[\frac{1 - \tau^{1/2} R_\rho}{2\left(1 - \tau^{1/2}\right)} \right]^{4/3} k \left(\frac{\alpha g}{\kappa \nu} \right)^{1/3} \Delta T^{4/3},$$

where $\lambda(\tau)$ is an empirical function of τ. Comparisons made here with data from Stamp *et al.* (1998) suggest that $\lambda(\tau) \approx 0.081$ for the salt–sugar system, which has $\tau \approx 0.33$, while comparisons with data from Turner (1965) suggest that $\lambda(\tau) \approx 0.075$ for the heat–salt system, which has $\tau \approx 0.01$. However, it may be that λ is additionally a function of the buoyancy ratio R_ρ, particularly as it affects the buoyancy frequency relevant to interfacial waves, which may enhance heat transfer across the interface. Evolution towards the steady states is rapid if R_ρ is not too close to $\tau^{-1/2}$, in which case the layered double-diffusive system can be considered as evolving through quasi-steady states even in situations in which the properties of the mixed layers are not held constant.

Extrapolations of the empirical relations determined for the heat flux by Huppert (1971) and by Marmorino & Caldwell (1976) by fitting results at low R_ρ give extremely poor results at high values of R_ρ (Newell 1984), where the present model works particularly well. The present model also provides a framework against which to discuss and analyse other processes that might operate in forced systems, particularly at low R_ρ. For example, the results presented in this paper give support to the idea (Linden 1974) that the interface is modified and perhaps completely disrupted by externally driven turbulence when such is present, for example in the experiments of Turner (1965) and of Marmorino & Caldwell (1976). If this is the case then the heat and salt fluxes may depend on both the strength and the structure of the turbulence in the mixed layers, which calls into question any simple parameterization of the fluxes that does not take explicit account of such turbulence.

The major conclusion of this paper is that double-diffusive interfaces are intrinsically time-dependent. In consequence, there is not a single mathematical expression that can be obtained for the heat flux across a double-diffusive interface, and fluxes can depend significantly on the initial conditions and the history of evolution. On the other hand, the model proposed in this paper is readily implemented numerically and runs extremely fast on a modern desk-top computer. The model provides a basis for future investigations of layered double-diffusive systems and could be extended to account for other processes (e.g. internal heating or shear) occurring in the mixed layers.

This work was begun while on sabbatical at the Applied Physics Laboratory of the University of Washington, where I was generously hosted by J. S. Wettlaufer, with whom I had many stimulating discussions. I have benefitted from many helpful

discussions with G. O. Hughes, H. E. Huppert, D. Leppinen, P. F. Linden, J. S. Turner and M. Ungarish. I am extremely grateful to G. O. Hughes and T. A. Newell for supplying data from their experiments.

REFERENCES

Ames, W. F. 1977 *Numerical Methods for Partial Differential Equations*, 2nd edn. Academic.

Castaing, B., Gunaratne, G., Heslot, F., Kadanoff, L., Libchaber, A., Thomae, S., Wu, X., Zaleski, S. & Zanetti, G. 1989 Scaling of hard thermal turbulence in Rayleigh-Benard convection. *J. Fluid Mech.* **204**, 1–30.

von Driska, P. M. 1982 Double-diffusive convection across a single thermohaline interface at high density stability ratios. Master's thesis, Mechanical Engineering, University of Illinois at Urbana-Champaign.

Fernando, H. J. S. 1989 Buoyancy transfer across a diffusive interface. *J. Fluid Mech.* **209**, 1–34.

Howard, L. N. 1964 Convection at high Rayleigh number. *Proc. 11th Intl Congr. Appl. Mech.*, pp. 1109–1115. Springer.

Huppert, H. E. 1971 On the stability of a series of double-diffusive layers. *Deep-Sea Res.* **18**, 1005–1021.

Huppert, H. E. 1986 The intrusion of fluid mechanics into geology. *J. Fluid Mech.* **173**, 557–594.

Huppert, H. E. & Turner, J. S. 1981 Double-diffusive convection. *J. Fluid Mech.* **106**, 299–329.

Linden, P. F. 1974 A note on the transport across a diffusive interface. *Deep-Sea Res.* **21**, 283–287.

Linden, P. F. 2000 Convection in the environment. In *Perspectives in Fluid Dynamics: a Collective Introduction to Current Research* (ed. G. K. Batchelor, H. K. Moffatt & M. G. Worster), pp. 289–345. Cambridge University Press.

Linden, P. F. & Shirtcliffe, T. G. L. 1978 The diffusive interface in double-diffusive convection. *J. Fluid Mech.* **87**, 417–432.

Marmorino, G. O. & Caldwell, D. R. 1976 Heat and salt transport through a diffusive, thermohaline interface. *Deep-Sea Res.* **23**, 59–67.

Newell, T. A. 1984 Characteristics of a double-diffusive interface at high stability ratios. *J. Fluid Mech.* **149**, 385–401.

Newell, T. A. & Boehm, R. F. 1982 Gradient zone constraints in a salt-stratified solar pond. *Trans. ASME: J. Solar Energy Engng* **103**, 280–285.

Schmitt, R. W. 1994 Double diffusion in oceanography. *Annu. Rev. Fluid Mech.* **26**, 255–285.

Shirtcliffe, T. G. L. 1973 Transport and profile measurements of the diffusive interface in double-diffusive convection with similar diffusivities. *J. Fluid Mech.* **57**, 27–43.

Stamp, A. P., Hughes, G. O., Nokes, R. I. & Griffiths, R. W. 1998 The coupling of waves and convection. *J. Fluid Mech.* **372**, 231–271.

Turner, J. S. 1965 The coupled turbulent transports of salt and heat across a sharp density interface. *Intl J. Heat Mass Transfer* **8**, 759–767.

Turner, J. S. 1974 Double-diffusive convection. *Annu. Rev. Fluid Mech.* **6**, 37–56.

Turner, J. S. 1979 *Buoyancy Effects in Fluids*. Cambridge University Press.

Turner, J. S. & Chen, C. F. 1974 Two-dimensional effects in double-diffusive convection. *J. Fluid Mech.* **63**, 577–592.